PROCEEDINGS OF SCIENCE

Radio measurements of air showers with the IceCube-Gen2 surface prototype station at the Pierre Auger Observatory

Stef Verpoest[a,*] **for the IceCube-Gen2**[1] **and Pierre Auger**[b,2] **Collaborations**

[a] *Bartol Research Institute, Department of Physics and Astronomy, University of Delaware, Sharp Lab, 104 The Green, Newark DE, 19716, United States of America*

[b] *Observatorio Pierre Auger, Av. San Martín Norte 304, 5613 Malargüe, Argentina*

E-mail: stef.verpoest@icecube.wisc.edu, analysis@icecube.wisc.edu, spokerspersons@auger.org

The design of the IceCube-Gen2 observatory, proposed as a next-generation extension of IceCube, includes a surface array consisting of scintillators and radio antennas. In addition to several such detectors already deployed at IceCube's surface array at the South Pole, a complete prototype station including three SKALA antennas has been operating at the Pierre Auger Observatory for several years. This setup has been used to successfully observe radio signals from air showers, demonstrated through coincident observations with the Auger Surface Detector. In this contribution, we present an updated analysis of these radio signals, and compare them to CoREAS simulations using the reconstruction from the Auger Surface Detector as input.

11th International Workshop on Acoustic and Radio EeV Neutrino Detection Activities (ARENA2026)
8-11 June 2026
Karlsruhe, Germany

[1] Full author list at https://icecube.wisc.edu/collaboration/authors.
[2] Full author list at https://www.auger.org/archive/authors_2026_06.html.
[*] Speaker

© Copyright owned by the author(s) under the terms of the Creative Commons Attribution-NonCommercial-NoDerivatives 4.0 International License (CC BY-NC-ND 4.0) All rights for text and data mining, AI training, and similar technologies for commercial purposes, are reserved. ISSN 1824-8039 . Published by SISSA Medialab.

PoS(ARENA2026)010

1. Introduction

The IceCube Neutrino Observatory [1] at the South Pole includes a surface air-shower detector, IceTop [2], which is being enhanced with scintillation detectors and radio antennas. The planned next-generation extension, IceCube-Gen2 [3], also foresees a surface array based on these detector types [4]. Prototype stations have been deployed at the South Pole [5, 6] and at the Pierre Auger Observatory [7] in Argentina, each featuring eight scintillator panels and three radio antennas of the SKALA v2 type [8]. The readout of the radio signals is triggered when six scintillator record a coincident signal. The station at Auger is located within the SD-433 area [9], the most densely instrumented part of the surface detector array. The successful detection of air-shower radio signals with this station, identified through coincident observations with the Auger SD-433 array, has been previously reported [10, 11]. In this contribution, we present an updated analysis including new data, and include a systematic comparison of the measured radio waveforms against CoREAS [12] simulations using the SD-433 shower reconstruction as input.

2. Identified Air Shower Events

The identification of air showers observed with the radio antennas of the prototype station, in coincidence with the Auger SD-433 array, was presented in earlier work [10, 11]. Here, we briefly summarize the selection procedure and present an updated sample. Starting from the scintillator-triggered events, the radio waveforms are processed, including corrections for DAQ artifacts, bandpass filtering to the 110 MHz to 185 MHz band, and the application of a frequency-weighting scheme to further suppress narrow-band background [13]. Using the signal-to-noise ratio (SNR) distributions obtained from background (fixed-rate trigger) waveforms, we select events with at least three high-SNR waveforms. For each selected event, a directional reconstruction is performed by fitting a planar shower front to the signal peak times in the antennas. The candidates are then matched to events reconstructed by the Auger SD-433 array [14] based on their trigger times and reconstructed arrival directions.

The present sample uses data recorded at a sampling rate of 800 Msps, collected between October 2023 and March 2024, and between April 2025 and October 2025. After removing periods of downtime due to hardware and software issues, this corresponds to a total runtime of 293.6 days. In total, 215 events with radio emission matching an event reconstructed by SD-433 were identified. Compared to the earlier analysis, an improved treatment of DAQ artifacts in the radio waveforms increased the rate of identified events by about 20%.

The reconstructed energies and arrival directions of the identified events are shown in Fig. 1, using values from the SD-433 reconstruction. Of the 215 matched events, 31 lack a successful SD-433 energy reconstruction and are excluded from the figures and further analysis; the remaining events span reconstructed energies from 33 PeV to 7 EeV. The arrival directions show the expected tendency towards larger angles to the geomagnetic field. The region around the zenith is excluded from the selection, as some residual DAQ artifacts can mimic vertical air showers.

PoS(ARENA2026)010

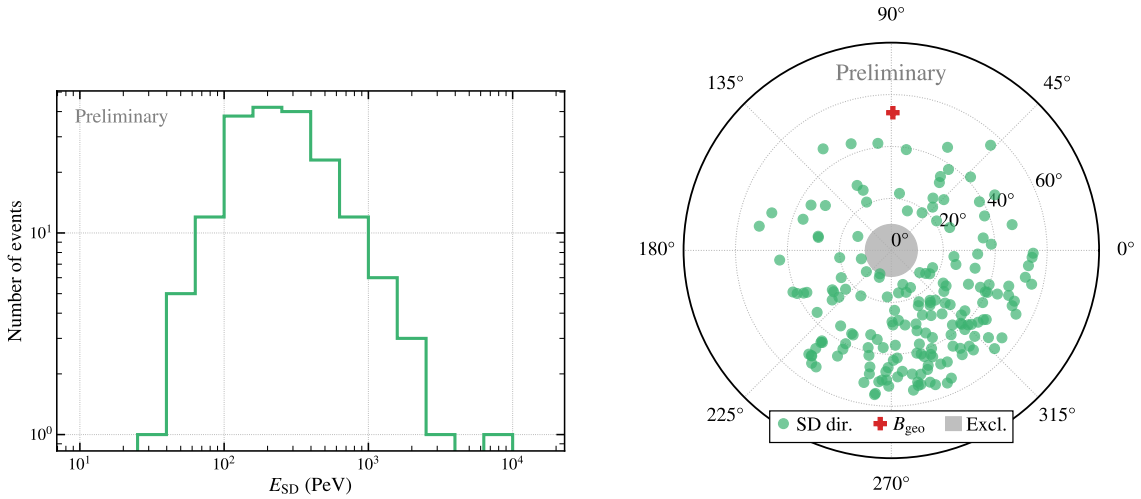

Figure 1: Properties of the identified air-shower events, as reconstructed by the Auger SD-433 array. Left: Distribution of the reconstructed shower energies (excluding 31 events without a successful SD-433 energy reconstruction). Right: Polar plot of the reconstructed arrival directions; the direction of the geomagnetic field is indicated, and the region around the zenith is excluded from the analysis.

3. Data–Monte Carlo Comparison

The sample of identified air showers is used to study the agreement between the observed radio signals and the expectations from simulations. For each event, dedicated simulations are produced, and observables are calculated that serve as proxies for the polarization of the radio signal. The method and results are detailed in the following. Before calculating any observables, all waveforms are upsampled by a factor 4 to 3.2 GSps by zero-padding in the frequency domain.

3.1 Goal and Method

The goal is to compare the properties of the simulated and observed radio signals. To this end, we compare the relative strength of the signals in the two polarization channels of each antenna. In this way, the comparison is largely insensitive to the missing absolute signal-chain calibration and to possible biases in the SD-433 energy estimate E_{SD}, while still providing a measure of the polarization of the electric field at each antenna.

We introduce the observable Q, comparing the signal power in the two channels of an antenna,

$$Q = \frac{S_0 - S_1}{S_0 + S_1}, \tag{1}$$

where $S_i = P_i^{\text{signal}} - P_i^{\text{noise}}$ is the noise-subtracted signal power in channel i, and the power is computed as

$$P_i = \sum_{t=t_{\text{peak}}-w}^{t_{\text{peak}}+w} V_i(t)^2 \tag{2}$$

in a window of half-width w around the signal peak. The value for w used here is 60 bins for the upsampled waveforms or 18.75 ns. The peak time is determined from the Hilbert envelopes $H_i(t)$ of

PoS(ARENA2026)010

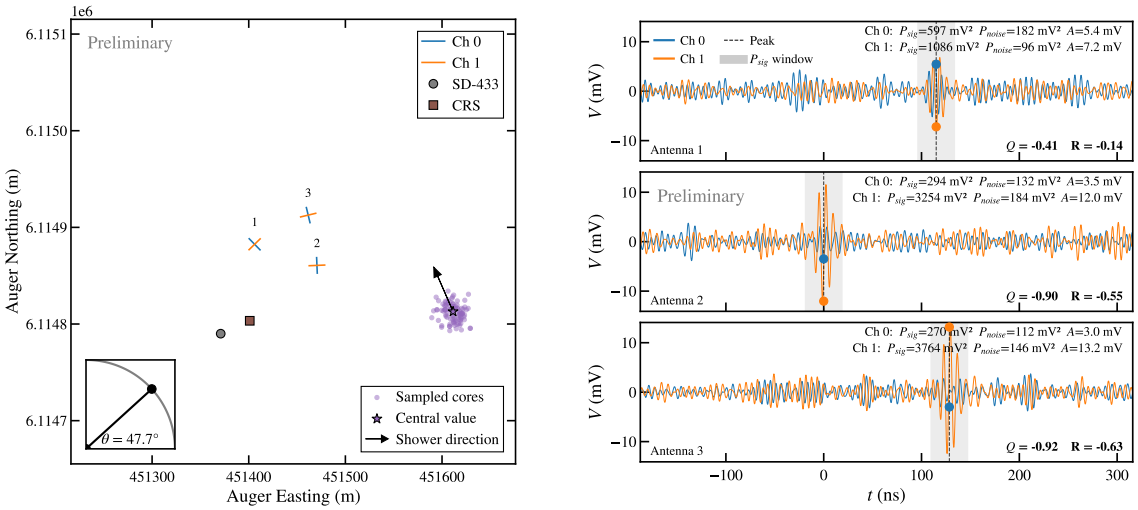

Figure 2: Illustration of the analysis for an example event. Left: The shower core reconstructed by SD-433, together with 100 core positions sampled according to the SD-433 reconstruction uncertainty (see Section 3.2), relative to the antenna positions. Right: Measured waveforms of one antenna used to compute the observables Q (Eq. (1)) and R (Eq. (3)), with the signal window indicated.

the two channels as $t_{\text{peak}} = \underset{t}{\text{argmax}} \left[H_0(t)^2 + H_1(t)^2\right]$. P_i^{noise} is evaluated by splitting the waveform into chunks of the same length as the signal window, excluding the identified signal window, and taking the median. By construction, $Q = +1$ (-1) if all power is contained in channel 0 (channel 1). The observable is similar to the normalized Stokes parameter Q/I, but defined in the antenna frame directly from the measured voltages rather than from the unfolded electric-field components.

We define an analogous observable R based on the amplitudes of the Hilbert envelopes,

$$R = \frac{A_0 - A_1}{A_0 + A_1}, \qquad A_i = \max_t \left(H_i(t)\right). \tag{3}$$

An example of the calculation is shown in Fig. 2 for a measured event.

For each identified air-shower event, the signal peaks are identified and Q and R are computed per antenna. The resulting distributions are shown in Fig. 3. The tendency for antennas 2 and 3 towards negative values is a result from their orientation which points roughly north, placing most of the signal in channel 1 for the majority of events. Antenna 1 is rotated by about 45° from this direction, resulting in more comparable signals in the two channels. Antenna 1 also contributes fewer events to the distributions, as it was non-operational during part of the data-taking period.

3.2 Simulations

To compare the measurements with expectations, a library of air-shower simulations is produced for each identified event. The showers are simulated with CORSIKA [15] and the radio emission with CoREAS [12], using the energy and direction from the SD-433 reconstruction as input, together with the geomagnetic field, observation level, and measured antenna positions of the Auger site. The Malargüe October atmosphere is used throughout; the use of a fixed atmosphere is a known limitation, and simulating the atmosphere specific to the time of each event is left for future work.

PoS(ARENA2026)010

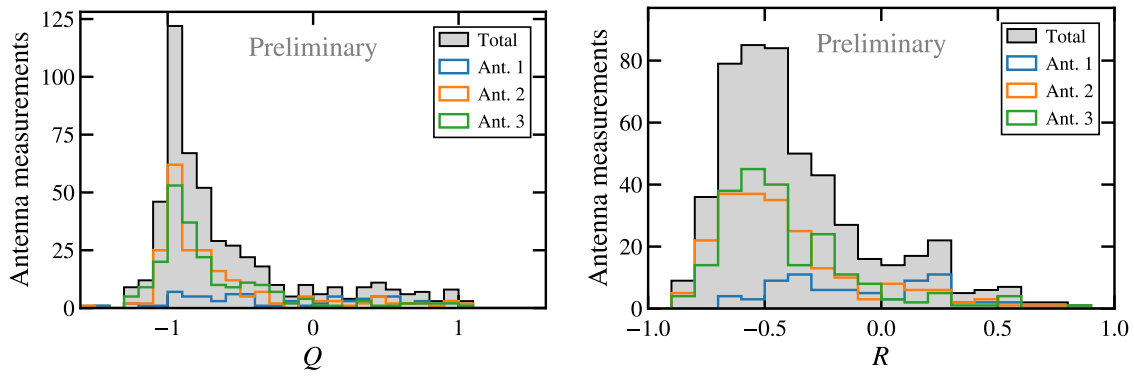

Figure 3: Distributions of the observables Q (left) and R (right) in data, calculated per antenna for the identified air-shower events.

The simulated radio signals are propagated through a simulation of the antenna and electronics response as implemented in the IceTray software framework [16].

The impact of the main sources of uncertainty are estimated based on dedicated simulation sets:

- **Longitudinal development:** for each event, 25 showers with proton primaries and 15 with iron primaries are simulated, covering the phase space of the longitudinal shower development, most importantly the position of the shower maximum $X_{\max}$.
- **Core position:** in addition to the central SD-433 value, 100 core positions are sampled following the SD-433 reconstruction uncertainty of each event (an example of the sampled cores is shown in the left panel of Fig. 2).
- **Background noise:** the simulation is repeated while injecting 100 different measured background waveforms, randomly selected within the same day as the actual event.
- **Antenna orientation:** the antenna orientations are perturbed 100 times following a Gaussian of 1° width. While differential-GPS measurements indicate a precision of 0.5° for the antenna alignment, we use a slightly more conservative value to guard against possible unknown biases or systematic uncertainties.

Uncertainties related to the calibration of the signal chain are not yet included.

The central value of each observable is taken from the noise-free simulations, as the median over the $X_{\max}$ distribution using the central core position and antenna orientation. The associated uncertainties are derived from the variation sets: a min–max range for $X_{\max}$, and 68% intervals for the core position, antenna orientation, and background noise. The median shift of the observables induced by noise is also taken into account. For most events, the noise variability is by far the dominant uncertainty.

3.3 Results

Simulations were produced for all identified air showers. The observables computed in data and simulation are compared in Fig. 4. Quality cuts are applied to the simulations, matching those

PoS(ARENA2026)010

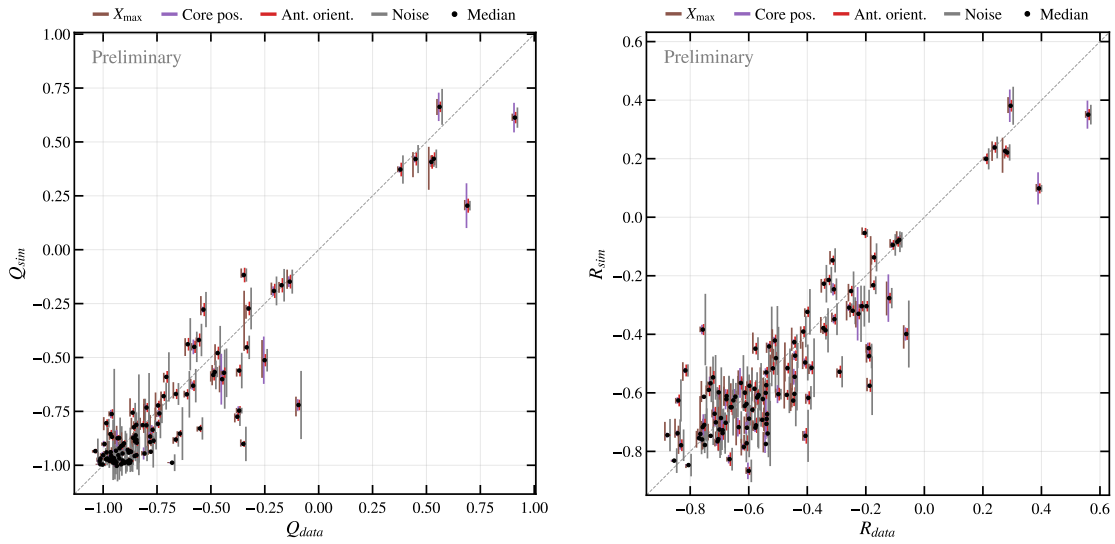

Figure 4: Comparison of the observables Q (left) and R (right) measured in data and predicted by simulations. Error bars are shown separately for the different sources of uncertainty considered (see Section 3.2 for details). Quality cuts were applied to select observations not dominated by background noise.

used for the data (per-channel SNR and directional-reconstruction requirements), together with an additional antenna-level cut on an SNR observable defined based on the total signal and noise power summed over both channels,

$$\mathrm{SNR}_P = \frac{P_0^{\mathrm{signal}} + P_1^{\mathrm{signal}}}{P_0^{\mathrm{noise}} + P_1^{\mathrm{noise}}}, \tag{4}$$

ensuring that the signal is not dominated by noise and that the peak is correctly identified ($\mathrm{SNR}_P > 4$). After these cuts, 115 antenna measurements from 70 unique events remain. The points generally lie along the diagonal, indicating agreement between data and simulation.

A more condensed view is provided by the pull distributions in Fig. 5, defined as the difference between the observable in data and simulation divided by the total uncertainty, with the individual contributions added in quadrature, $\sigma^2_{\mathrm{tot}} = \sigma^2_{X_{\mathrm{max}}} + \sigma^2_{\mathrm{core}} + \sigma^2_{\mathrm{orient}} + \sigma^2_{\mathrm{noise}}$. For a consistent description of the data within the estimated uncertainties, the distribution is expected to be normal, which holds for the bulk of the antenna measurements. However, outliers at large values are present, and an unbinned maximum-likelihood fit indicates a possible bias ($\mu_Q = 0.88 \pm 0.22$, $\mu_R = 0.49 \pm 0.19$) and an underestimation of the uncertainties ($\sigma_Q = 2.3 \pm 0.3$, $\sigma_R = 2.0 \pm 0.2$). We verified that these outliers are not removed by applying stricter SD-433 quality cuts, which additionally restrict the sample to zenith angles below 45°. With these cuts, 62 data points remain, yielding $\mu_Q = 0.59 \pm 0.23$, $\sigma_Q = 1.8 \pm 0.2$ and $\mu_R = 0.29 \pm 0.22$, $\sigma_R = 1.8 \pm 0.3$.

We conclude that for the majority of the events, the polarization of the air-shower signals is well described by the simulations, and that our simulated signal chain provides a reasonable description of reality. Outlier events and the best-fit width of the pull distribution being larger than unity may result from various effects not yet included in our study, such as atmospheric effects and signal-chain calibration uncertainties. These aspects will be studied in more detail in future work.

PoS(ARENA2026)010

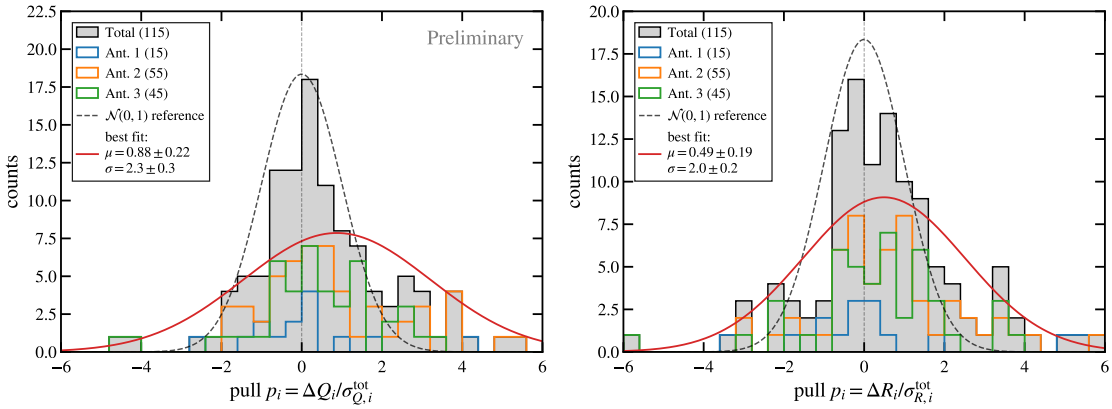

Figure 5: Pull distributions of the observables Q (left) and R (right), shown for the three antennas. The pull is the difference between data and simulation divided by the total uncertainty. A consistent description within the uncertainties would yield a standard normal distribution (indicated).

4. Conclusion

A prototype station of the IceCube-Gen2 surface array has been operating at the Pierre Auger Observatory for several years, providing a growing sample of air showers observed with its radio antennas, and recent improvements in the low-level data processing have increased the efficiency of the event identification. For the updated sample of identified air showers presented in this work, a dedicated simulation library was produced, including variations describing several sources of possible disagreement between data and simulations: the longitudinal shower development, the variability of the background noise, the shower core position, and the antenna orientation.

Using two observables that serve as proxies for the polarization of the electric field at the antennas (Eqs. (1) and (3)), we performed a systematic comparison between data and simulation. We find reasonable overall agreement, albeit with possible indications of an incomplete uncertainty budget. For a more complete understanding of these results, follow-up studies of the impact of atmospheric conditions and of the uncertainties in the antenna model and signal-chain calibration will be performed.

References

[1] **IceCube** Collaboration, M. G. Aartsen *et al.*, *JINST* **12** no. 03, (2017) P03012. [Erratum: JINST 19, E05001 (2024)].

[2] **IceCube** Collaboration, R. Abbasi *et al.*, *Nucl. Instrum. Meth. A* **700** (2013) 188–220.

[3] **IceCube-Gen2** Collaboration, M. G. Aartsen *et al.*, *J. Phys. G* **48** no. 6, (2021) 060501.

[4] **IceCube-Gen2** Collaboration, F. G. Schroeder *et al.*, *PoS* **ICRC2021** (2021) 407.

[5] **IceCube** Collaboration, R. Abbasi *et al.*, *PoS* **ICRC2021** (2021) 314.

[6] **IceCube** Collaboration, A. Rehman *et al.*, *PoS* **ICRC2023** (2023) 291.

PoS(ARENA2026)010

[7] **Pierre Auger** Collaboration, A. Aab *et al.*, *Nucl. Instrum. Meth. A* **798** (2015) 172–213.

[8] E. de Lera Acedo *et al.*, "Evolution of skala (skala-2), the log-periodic array antenna for the ska-low instrument," in *2015 International Conference on Electromagnetics in Advanced Applications (ICEAA)*, pp. 839–843. 2015.

[9] **Pierre Auger** Collaboration, P. Abreu *et al.*, *PoS* **ICRC2021** (2021) 224.

[10] **IceCube-Gen2** and **Pierre Auger** Collaborations, S. Verpoest *et al.*, *PoS* **ARENA2024** (2024) 037.

[11] **IceCube-Gen2, Pierre Auger** Collaboration, S. Verpoest *et al.*, *PoS* **ICRC2025** (2025) 428.

[12] T. Huege, M. Ludwig, and C. W. James, *AIP Conf. Proc.* **1535** no. 1, (2013) 128.

[13] **IceCube** Collaboration, R. Abbasi *et al.*, *PoS* **ICRC2021** (2021) 317.

[14] **Pierre Auger** Collaboration, G. Brichetto Orquera *et al.*, *PoS* **ICRC2023** (2023) 398.

[15] D. Heck *et al.*, *Forschungszentrum Karlsruhe Report FZKA-6019* (1998) .

[16] **IceCube** Collaboration, R. Abbasi *et al.*, *JINST* **17** no. 06, (2022) P06026.

Acknowledgments

We thank Eloy de Lera Acedo and Quentin Gueuning for their support regarding the SKALA v2 antennas. This project benefited from funding provided by the European Research Council (ERC) and the U.S. National Science Foundation (NSF). Further acknowledgments are included with the full author lists at: https://www.auger.org/archive/authors_2026_06.html and https://icecube.wisc.edu/collaboration/authors/.

PoS(ARENA2026)010